Analysis of coupling between two sub-machines in co-axis dual-mechanical-port flux-switching PM machine for fuel-based extended range electric vehicles

Lingkang Zhou[1], Wei Hua[1*], Zhongze Wu[2], Xiaofeng Zhu[1], Fangbo Yin[1]

[1] School of Electrical Engineering, Southeast University, Si-Pai-Lou No. 2, Nanjing, China
[2] Department of Mechanical Engineering, University of Bath, Bath, BA2 7AY, UK
[*]huawei1978@seu.edu.cn

Abstract: The permanent magnet (PM) field coupling between inner and outer machines of co-axis dual-mechanical-port flux-switching permanent magnet (CADMP-FSPM) machines is investigated. Firstly, the relationships between the inner and outer stator teeth are analytically evaluated, with three key stator teeth types defined, i.e. series, parallel, and independent teeth. Secondly, the negative effects of PM field coupling, including high even-order electromotive force (EMF) harmonics, three-phase EMFs asymmetry and DC bias component in flux-linkages, are investigated and verified by two CADMP-FSPM machines, namely, 5/6-12/22, and 5/6-18/42 structures. It is found that for avoiding the negative effects of PM field coupling, all inner and outer stator teeth types should be the same, thus, a 10/12-12/22 structure CADMP-FSPM machine is introduced for analysis. Thirdly, the performance of the 10/12-12/22, 5/6-12/22, and 5/6-18/42 structures, featured by PM field distributions, d-axis flux-linkage ripples, cogging torques, electromagnetic torques, losses and efficiencies, are comparatively analysed by finite element (FE) analysis. The results indicate that the 10/12-12/22 structure exhibits the lowest PM field coupling level and the best performance. Moreover, the 10/12-12/22 structure can avoid all the negative effects of PM field couplings. A prototyped 10/12-12/22 CADMP-FSPM machine is built and tested to verify the FE predicted results.

1. Introduction

The fuel-based extended range electric vehicle (ER-EV) is proposed in [1], as a transition from current engine vehicles to the pure electric vehicles (PEVs), where the power system is comprised of battery packs, a traction motor, a generator and an internal combustion engine (ICE). The extender and the traction motor in the conventional ER-EVs are independent mechanically, and the extender is comprised of an ICE and a generator. Consequently, the traction motor and the extender can be laterally placed in the front of the conventional ER-EVs together or placed at both ends of the vehicles respectively [2], [3]. Both of these two layouts cause space consumption and heat dissipation problems. To overcome these disadvantages, a co-axis dual-mechanical-port flux-switching permanent magnet (FSPM) (CADMP-FSPM) machine is proposed in [4] to combine the generator and traction machine together, thus, the utilization of space is improved. FSPM machine [5] is a typical stator-PM machine operating based on magnetic gearing effect [6], in which both the PMs and armature windings are placed in the stator whilst the rotor is very simple without any PM or coil [7], [8].

So far, the main focus on CADMP-FSPM machines are the structural optimization, performance analysis, and power distribution [4], [9]. The PMs field coupling phenomena of a 10-inner-rotor-pole/12-inner stator-slot-12-outer-stator-slot/22-outer-rotor-pole (10/12-12/22) CADMP-FSPM machine was introduced and a mechanical decoupling method was given in [4].

This paper will focus on the PM field coupling of a CADMP-FSPM machine with different stator teeth collocations. On this basis, the optimal stator teeth numbers of inner and outer machines will be given. In the following, firstly, machine topology and operation principle are introduced in section II. In section III, three stator teeth types which can contain all the PM field coupling situations are defined according to the space and magnetization directions. The effects of PM field coupling, including high even-order EMF harmonics, three-phase EMFs asymmetry and DC bias component in flux-linkages, will be investigated and verified by two CADMP-FSPM machines, namely, 5/6-12/22 and 5/6-18/42 structures. It will be found that all the stator teeth types of both inner and outer machines should be the same. On this basis, the recommended stator teeth numbers of both inner and outer machines are given and then a 10/12-12/22 structure CADMP-FSPM machine is introduced for verifying. Thereafter, in section IV, the PM field coupling levels, including PM field distributions, and *d*-axis flux-linkage ripples, cogging torques, electromagnetic torques, losses and efficiencies, of three CADMP-FSPM machines above will be analysed and evaluated. In section V, the CADMP-FSPM prototype will be built and tested to verify the finite element (FE) predicted results, followed by conclusions in section V.

2. Machine topology and principle

The CADMP-FSPM machine topology is shown in Figs. 1(a) and (b), which is comprised of an inner-rotor machine and an outer-rotor machine co-axially accommodated, and separated by a non-magnetic ring. Both inner and outer machines are FSPM machines, whilst the inner and outer stators are connected back to back through a non-magnetic ring.

The CADMP-FSPM machine-based powertrain structure for ER-EVs is shown in Fig. 1(c). It can be seen that the powertrain is constructed by a CADMP-FSPM machine, two DC/DC modules, two converter modules and a battery pack. The inner rotor is normally connected to the ICE directly, whilst the outer rotor is normally connected to the

final reduction gear. The battery packs absorb or provide energy from or to the DC bus. The outer machine operates as a traction motor to drive the vehicle and absorb the energy from the battery packs.

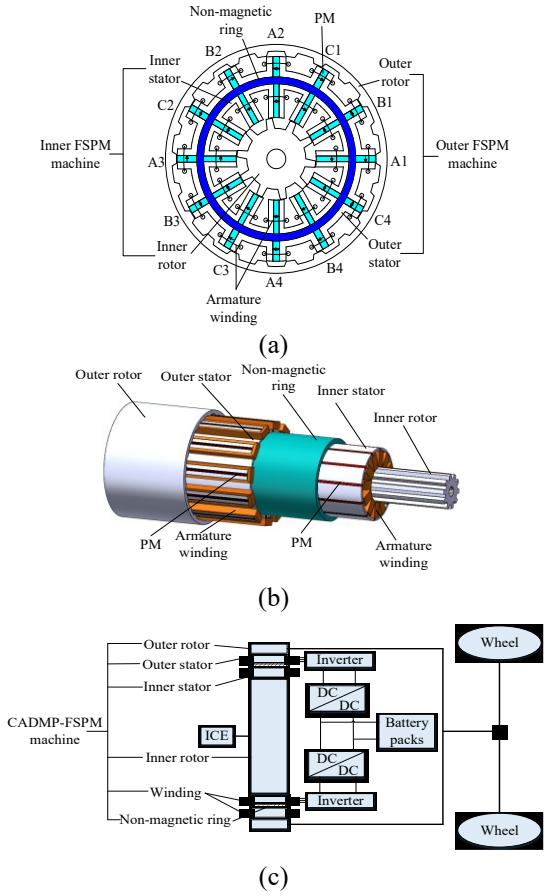

Fig. 1 *The configuration of a three-phase CADMP-FSPM machine and structure of the CADMP-FSPM machine-based powertrain for ER-EVs.*
(a) 2D Cross section ***(b)*** 3D topology. ***(c)*** Powertrain

3. Effects of PM field coupling

The PMs field coupling will cause three major effects as follows: 1) High EMF distortions. 2) Three-phase EMFs asymmetry. 3) Flux-linkage DC bias component.

Briefly, as all PMs are sandwiched between two U-type stator teeth, it can be expected that the PM field coupling due to magnets in both stators is directly related to the stator teeth collocation, the rotor positions, and the magnetization directions of PMs. Thus, it is necessary to analyse the relationships between stator teeth collocation and PM field coupling effects, to find out the recommended inner and outer stator teeth combination.

Through a simple geometric derivation, the inner and outer stator teeth relationships can be concluded as follows: 1) Two stator teeth are in line radially and the magnetization directions of two pieces of PMs are same as shown in Fig. 2(a), therefore, these stator teeth are defined as parallel teeth since the magnetic circuits are parallel, and the PMs are called parallel PMs. 2) Two stator teeth are in line radially but the magnetization directions of two pieces of PMs are opposite as shown in Fig. 2(b), therefore, these stator teeth are defined as series teeth since the magnetic circuits are series, and the PMs are called series PMs. 3) One stator tooth is in line radially with the other stator slot between two stator teeth as shown in Fig. 2(c), therefore, this stator tooth are defined as an independent tooth, and the PMs are called independent PMs. Moreover, the teeth number of the outer machine is larger than that of the inner one due to geometric reasons. According to the well-known "minimum reluctance principle", two series PMs in Fig. 2(b) form one type series magnetic circuit which can be defined as series-series-type (SS-type) series magnetic circuits. Also, two independent teeth with different magnetization directions in Fig. 2(c) form the other type series magnetic circuit which can be defined as parallel-independent-type (PI-type) series magnetic circuits.

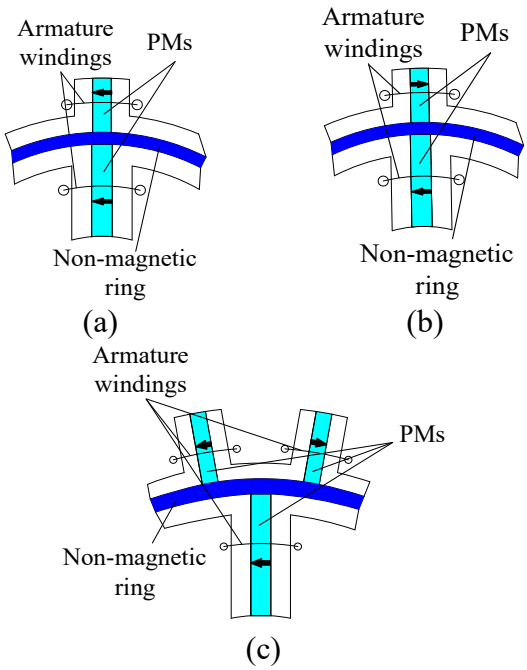

Fig. 2 *Three stator teeth types of the CADMP-FSPM machine.*
(a) Parallel teeth ***(b)*** Series teeth. ***(c)*** Independent teeth

Both inner and outer rotor pole numbers can be determined as [10], [11], [12]:

$$P_r = P_s\left(2 \pm \frac{k}{2m}\right) \tag{1}$$

where, P_r and P_s are the rotor pole number and stator slots number of the FSPM machine respectively, m is phase number, and k is a positive integer. For a quantitative analysis, key dimensions of the exampled CADMP-FSPM machine are given in Table I.

Table I Key Dimensions of the exampled CADMP-FSPM Machines

Key Dimensions	Inner machine	Outer machine
Rotor outer diameter	12 mm	128 mm
Stator outer diameter	87.6 mm	115.78 mm
Rotor inner diameter	42.2 mm	116.48 mm
Stator inner diameter	42.9 mm	92.6 mm
Non-magnetic ring thickness	5 mm	
Axis length	75 mm	75 mm

3.1. Even-order EMF Harmonics

If we suppose that the inner stator teeth of the CADMP-FSPM machine consist of series teeth and parallel teeth, then it can be deduced that the outer stator teeth consist of series teeth, parallel teeth and independent teeth. This is due to the fact that the magnetization direction of adjacent stator teeth PMs in FSPM machines is opposite to each other.

Therefore, SS-type series magnetic circuits and PI-type series magnetic circuits will be formed if CADMP-FSPM machine contains series teeth and independent teeth, both of two types series magnetic circuits cause extra magnetic flux leakages. The magnetic flux leakages caused by PI-type series magnetic circuits are less than SS-type as the PI-type series magnetic circuits have a larger magnetic resistance. The flux leakage difference will cause high even harmonic components and thus a high EMF distortion.

A 5/6-12/22 structure CADMP-FSPM machine shown in Fig. 3(a) is adopted for example. As can be seen, the inner stator teeth of 5/6-12/22 structure consists of parallel teeth and series teeth, whilst the outer stator teeth are consisted of parallel teeth, series teeth and independent teeth. The inner series teeth a2 and outer series teeth A3 form SS-type series magnetic circuits as path1. The inner parallel teeth a1 has formed PI-type series magnetic circuits with outer independent teeth B1 and C4 as path2. Since the flux leakage caused by path1 is higher than path2, EMF of inner phases suffer from high even-order harmonics.

On the other hand, taking outer phase A as an example, the flux of teeth A1 and A2 is large, because teeth C4 and B2 can contribute their flux to teeth A1 and A2 sides, respectively. The flux of tooth A4 is low as tooth B4 cannot contribute its flux as series teeth. The flux of tooth A3 is also low due to series teeth. Due to the complementarity and consistency of windings [10], EMF of outer phase A suffers from a much lower even harmonic component than inner phase A.

The phase EMF relative values of individual harmonics and waveforms of both inner and outer machines are shown in Figs. 3(b) and (c), respectively. As can be seen, both inner and outer phase EMFs form symmetrical three-phase systems of EMFs due to the same three-phase flux leakage. The second harmonic component of inner phase A EMF is extremely high, i.e. 26%. However, the second harmonic of outer phase A EMF is much lower than that of the inner machine, which confirms the previous analysis.

3.2. EMF asymmetry

The amplitudes of EMFs will be influenced by flux leakage. Supposing that the stator teeth types of phases A and B are different and thus cause different flux leakages, then, it can be deduced that the amplitudes of flux-linkages and EMFs of phase A and B are different, which will cause asymmetry between phase EMFs.

A 5/6-18/42 structure CADMP-FSPM machine shown in Fig. 4(a) is adopted for example. As can be seen, all the inner stator teeth are parallel teeth. The outer phase A stator teeth are also parallel teeth. However, the outer stator teeth of outer phases B and C are all independent teeth. Moreover, all outer independent teeth which belong to outer phases B and C have formed PI-type series magnetic circuits with inner parallel teeth as path3 in Fig. 4(a). Whereas, all outer phase A parallel teeth have not formed any series magnetic circuits with inner stator teeth. Thus, the amplitudes of EMFs of phase A and B or C are different, as shown in Fig. 4(b). In addition, the EMF waveforms of phases B and C are symmetric as their flux leakages are similar. The inner three-phase EMFs form a symmetrical three-phase system of EMFs, as all inner stator teeth are parallel teeth and thus have similar flux leakages.

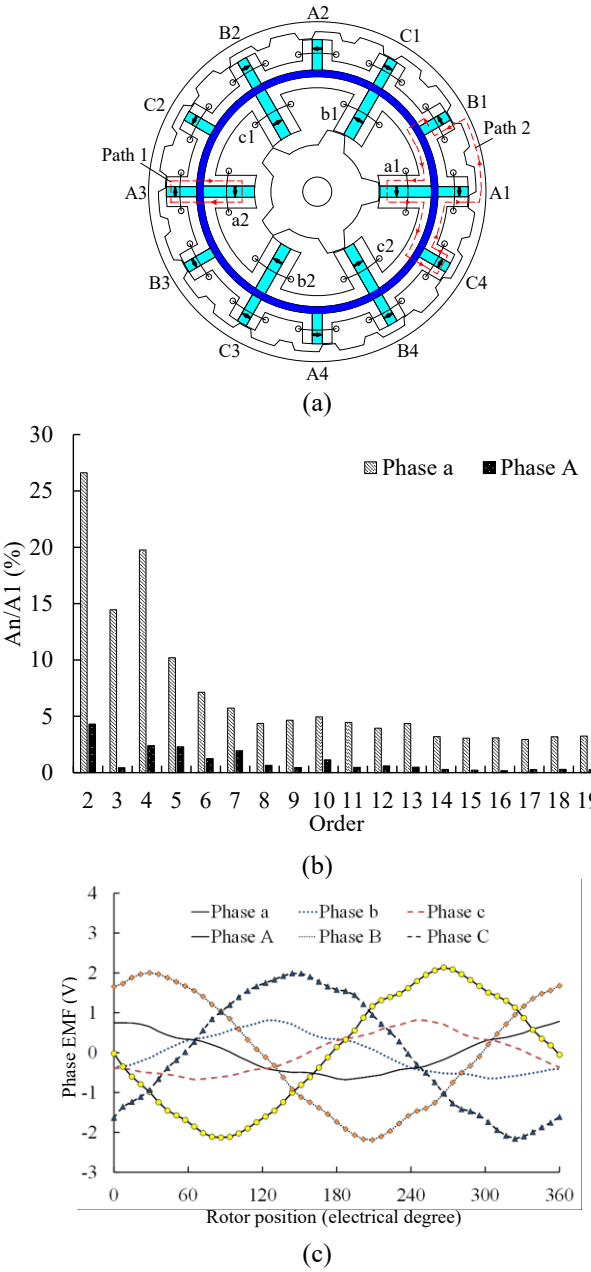

Fig. 3 *The configuration and EMF performance of a 5/6-12/22 CADMP-FSPM machine.*
(a) Configuration. ***(b)*** Relative values of individual harmonics. ***(c)*** Waveforms.

3.3. Flux-linkage DC bias component

The flux leakage is caused by series magnetic circuit and influences phase flux-linkage. Supposing the flux of the series magnetic circuit which flows through the phase coils is unidirectional, DC bias components are expected to exist in the flux-linkages of the phase.

A 5/6-18/42 structure CADMP-FSPM machine shown in Fig. 4(a) is still adopted for example. For the inner machine, taking inner stator tooth a1 as an example, tooth a1 forms a PI-type series magnetic circuit with two independent outer stator teeth B1 and C6 as path 3. The flux of the PI-type series magnetic circuit through coil a1 is bidirectional, where the inflow and outflow of PM fluxes are equal. Therefore, inner stator tooth a1 causes the magnetic leakage, but it does not contain a DC bias component. However, for coils B1 and C4, the PI-type series magnetic circuits flux flows through them

unidirectional, DC bias components are expected to exist in the flux-linkages of phases B and C in the outer machine. Similarly, the inner stator tooth b1, c1 and etc. also form the PI-type series magnetic circuits with the nearest independent outer stator teeth. The inner and outer three-phase flux-linkages are shown in Fig. 4(c). As can be seen, the flux-linkages of outer phases B and C contain a DC bias component, whereas, the outer phase A flux-linkage has no DC bias component as its stator teeth are parallel teeth and do not form any series magnetic circuits with inner machine.

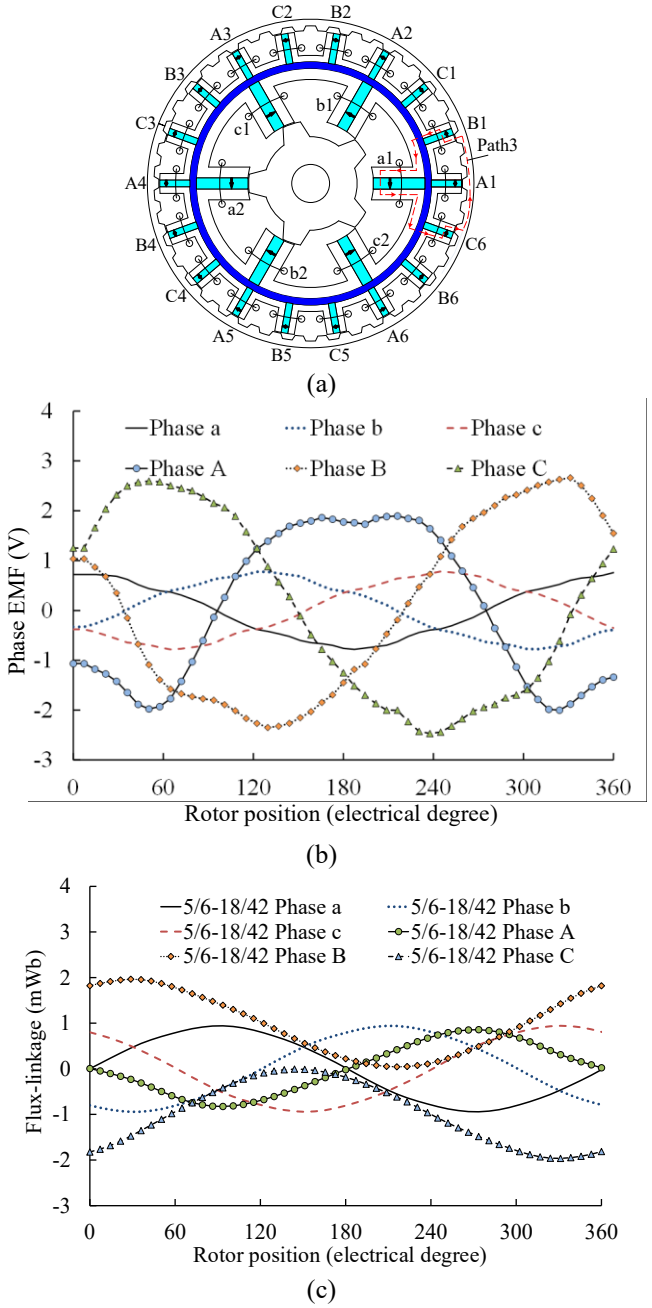

Fig. 4 *The configuration and performance of a 5/6-18/42 CADMP-FSPM machine.*
(a) Configuration. ***(b)*** EMFs. ***(c)*** Flux-linkages.

3.4. Recommended stator teeth collocations

From the above analysis, the flux leakage level is significantly affected by the stator teeth types. If stator teeth types that belong to one phase are different, even-order harmonics are generated in the EMF due to the distinct flux leakage. The EMF asymmetry is produced if stator teeth types of different phases are different. Series and independent teeth cause extra flux leakages, moreover, flux-linkage DC bias component will be caused by the unidirectional flux of the series magnetic circuit. Therefore, the inner and outer stator teeth types should both be parallel teeth to avoid EMF even-order harmonics, EMF asymmetry and flux-linkage DC bias component. On this basis, the recommended teeth collocations can be summarized as follows: P_{ri}/P_s-P_s/P_{ro}, where, P_{ri} and P_{ro} are inner and outer stator poles, respectively, P_s is stator teeth numbers of both inner and outer machines.

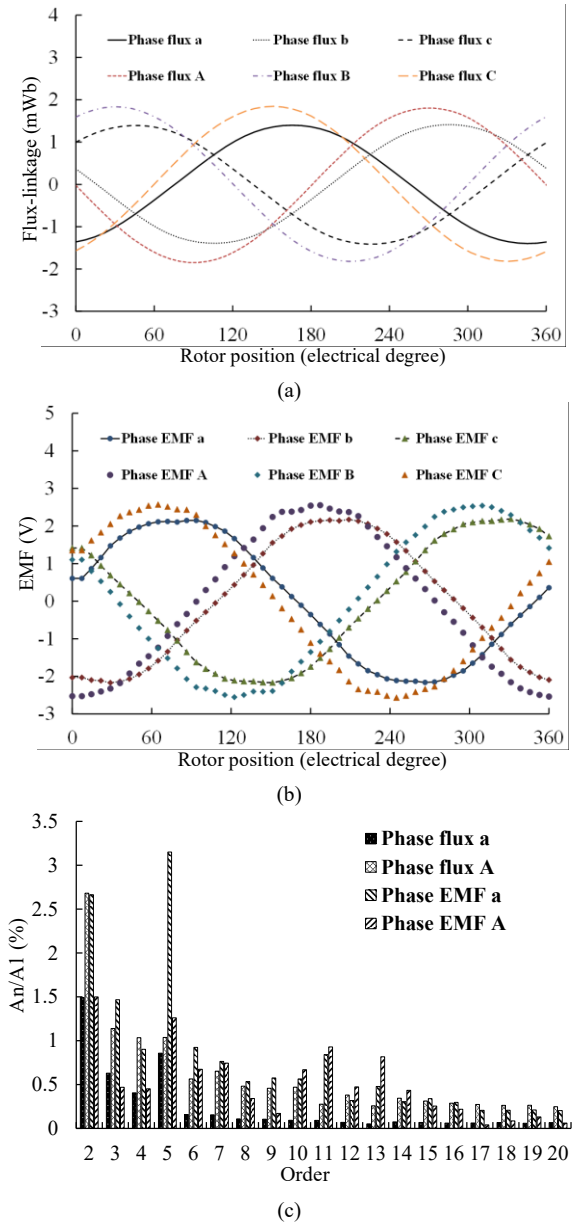

Fig. 5 *The flux-linkages and EMFs of the 10/12-12/22 CADMP-FSPM machine.*
(a) Flux-linkages. ***(b)*** EMFs. ***(c)*** Relative values of individual harmonics.

The 10-inner-rotor-pole/12-inner stator-slot FSPM machine is a typical structure [10] and the 22-inner-rotor-pole/12-inner stator-slot outer rotor FSPM machine is also an optimal structure [11]. Thus, a 10/12-12/22 structure

CADMP-FSPM machine, which is shown in Fig. 1(a), is adopted for example. Its inner and outer phase flux-linkages and EMFs are shown in Fig. 5. As can be seen, both inner and outer flux-linkages and EMFs are symmetrical and do not contain any DC component, the relative values of individual harmonics of inner and outer flux-linkages and EMFs are also significantly low.

4. Electromagnetic performance

The PM coupling effects will cause serious performance reductions. To further investigate the PM field coupling influences, the detailed PM field distributions, *d*-axis flux-linkage ripples, cogging torques, electromagnetic torque ripples and losses of the above mentioned 10/12-12/22, 5/6-12/22, and 5/6-18/42 structures are analyzed and compared in this section. All three machines are optimized.

4.1. PM field distributions

Because all three CADMP-FSPM machines are symmetrical, the open-circuit PM field distributions diagram of the half structure of three machines are displayed from Figs. 6(a) to (c). As can be seen, the inner and outer series teeth in a radial line form series magnetic circuits as path1 causes serious flux leakages. The outer independent stator teeth of the 5/6-12/22 and 5/6-18/42 structures form series magnetic circuits with nearest inner parallel stator teeth as path2 and path 3 also cause flux leakages. The 10/12-12/22 structure contains no series magnetic circuit as the number of inner and outer stator teeth is equal and the teeth are parallel.

The PMs field coupling levels can be evaluated by comparing the flux lines passing through the non-magnetic ring. The flux densities in the non-magnetic rings of three machines are calculated by FEA, as shown in Fig. 6(d). From Fig. 6(d), the 10/12-12/22 structure exhibits the lowest coupling and the amplitude, i.e. only 0.15T, whereas the 5/6-12/22 structure has the highest level and the amplitude is 0.7T. The 5/6-18/42 structure has medium coupling and the amplitude is 0.65T. Because the flux leakage caused by series stator teeth are higher than independent stator teeth and parallel stator teeth which confirms the analysis above.

4.2. D-axis flux-linkage ripple

Due to the accumulation effect of FSPM machines, the inner and outer *d*-axis PM flux linkages of three CADMP-FSPM machines will be rippled versus relative positions between inner and outer rotors [13]. The magnetic coupling can be quantified by evaluating the *d*-axis PM flux pulsations of one machine when the other machine rotates only. The PM flux ripple k_{ripple} is defined as,

$$k_{ripple}=\varphi_{p\text{-}p}/\varphi_{ave} \quad (2)$$

where, $\varphi_{p\text{-}p}$ and φ_{ave} are peak-peak (P-P) and average *d*-axis flux-linkage values, respectively, where one rotor is static, while the other one is rotating.

The *d*-axis flux average values and ripples for the inner and outer machines of the three analyzed CADMP-FSPM structures are shown in Figs. 7(a) and (b), respectively. From Fig 7(a), as the PM numbers are equal, the *d*-axis flux average values of inner machines of 5/6-12/22 and 5/6-18/42 structures are roughly the same, whereas that of the 10/12-12/22 structure is higher. Similarly, the *d*-axis flux average values of 18/42 outer machine is the highest. The *d*-axis flux average values of 5/6-12/22 structure is lower than 10/12-12/22 structure as flux leakages. Thus, it can be concluded that the *d*-axis average flux value is larger when the flux leakage is lower, also the average flux value is larger when more PMs are mounted.

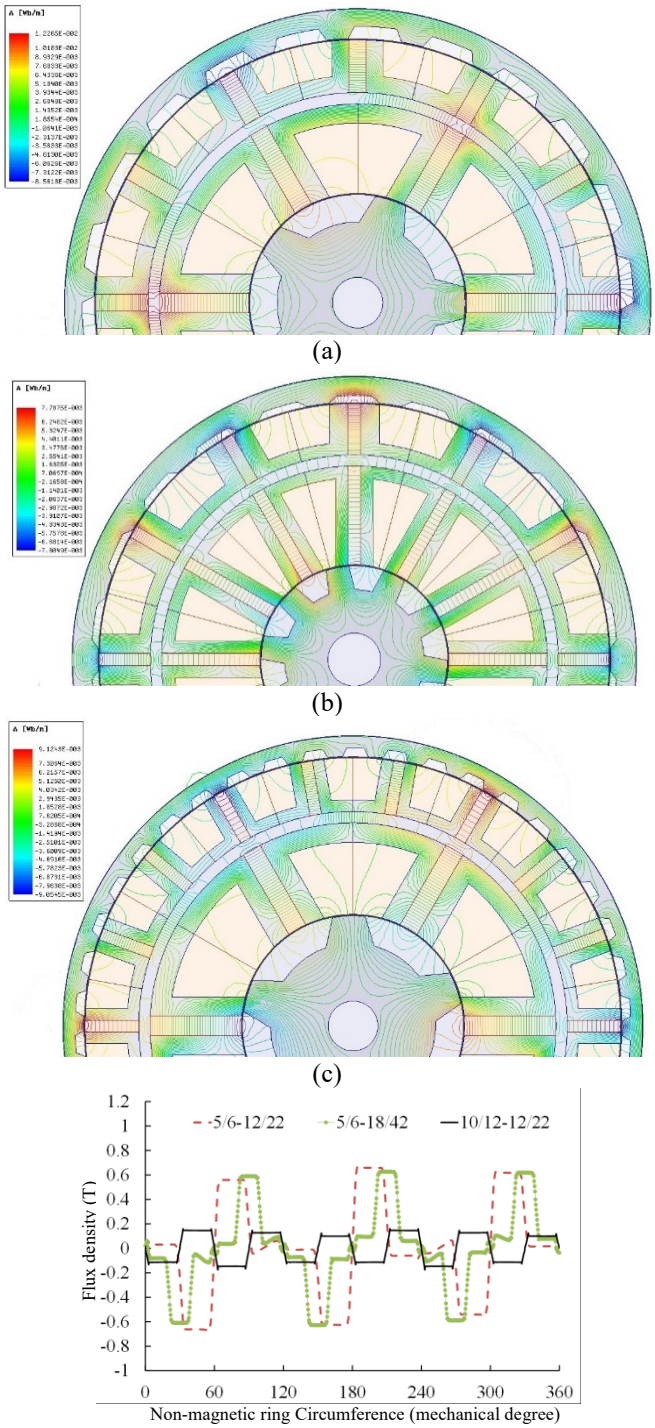

Fig 6 *The open-circuit PM field distributions and medium non-magnetic ring flux densities of three CADMP-FSPM machines.*
(a) 5/6-12/22. ***(b)*** 10/12-12/22. ***(c)*** 5/6-18/42. ***(d)*** Flux densities.

From Fig 7(b), The inner and outer *d*-axis flux-linkage ripples of 5/6-12/22 structure are the highest as the saturation of both inner and outer machines are the lowest. On the other hand, the inner machine *d*-axis flux-linkage ripple of 10/12-12/22 structure is the lowest as its inner machine features the highest saturation. Similarly, the outer machine *d*-axis flux-linkage ripple of 5/6-18/42 structure is the lowest as its outer machine features the highest saturation. Thus, it can be calculated that the *d*-axis flux-linkage ripple is lower when the machine saturation is higher.

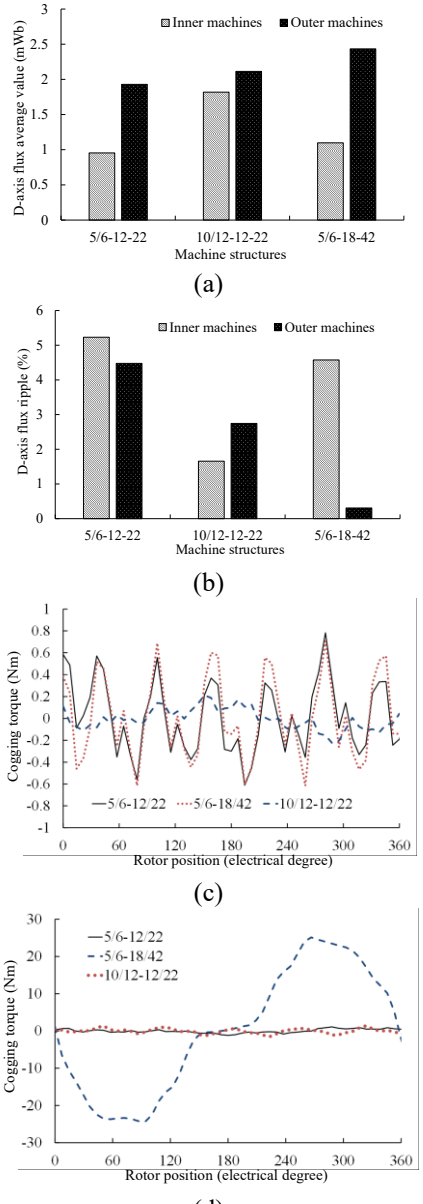

Fig. 7 *D-axis PM flux-linkage and cogging torques of the three CADMP-FSPM machines.*
(a) Average values. ***(b)*** Ripples. ***(c)*** Inner machine. ***(d)*** Outer machine.

4.3. Cogging torque

The inner and outer cogging torque waveforms of three machines are shown in Figs. 7 (c) and (d), respectively. Moreover, both inner and outer cogging torque peak-to-peak (P-P) values of three machines are shown in Fig. 8 (a).

Among the inner machines, the 10/12-12/22 structure features the lowest P-P value. Moreover, the P-P value of 5/6-12/22 and 5/6-18/42 structures are roughly same.

Among the outer machines, due to the PI-type series magnetic circuits of 5/6-18/42 structure as path3, the outer machine sucks magnetic flux of inner machine through the outer air-gap, which means the magnetic field of outer machine is enhanced by inner machine. Thus, the P-P cogging torque of 5/6-18/42 structure is much higher than the other two structures. On the other hand, due to the PI-type series magnetic circuits of 5/6-12/22 structure as path2, the outer machine sucks magnetic flux of inner machine through the outer air-gap and enhance the outer magnetic field. However, the SS-type series magnetic circuits of 5/6-12/22 structure as path1 cause serious flux leakage, the outer magnetic field is greatly reduced. Moreover, the flux leakage caused by SS-type series magnetic circuits is higher than PI-type series magnetic circuits. Thus, the P-P cogging torque of the 5/6-12/22 structure is slightly lower than the 10/12-12-22 structure.

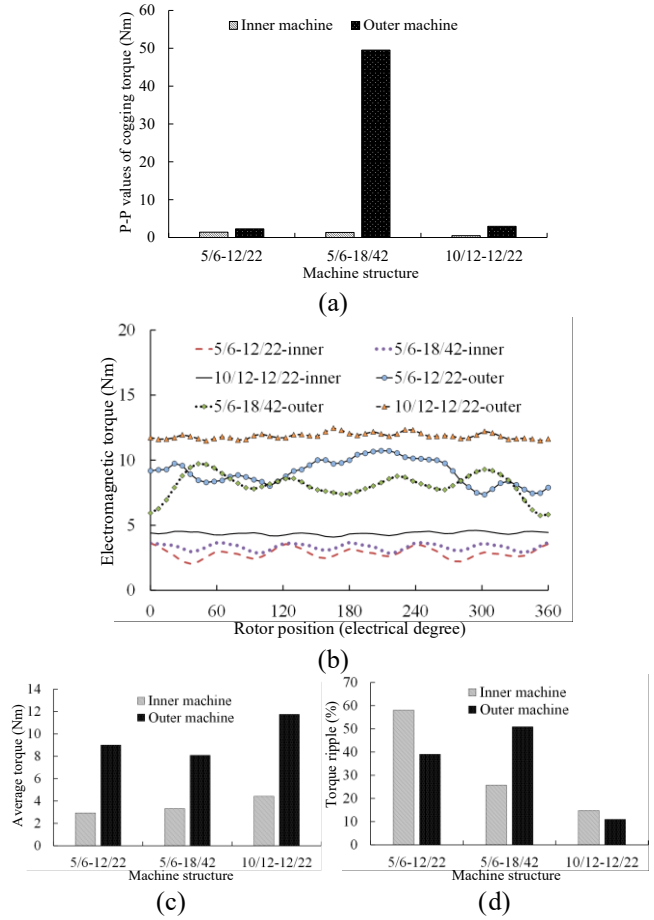

Fig. 8 *Cogging torques P-P values, ripples and average values of electromagnetic torques of three CADMP-FSPM machines.*
(a) P-P values of cogging torques. ***(b)*** Waveforms. ***(c)*** Average values of electromagnetic torques. ***(d)*** Ripples of electromagnetic torques.

4.4. Electromagnetic torque

For quantitative analysis, the current density and slot filling factors of three machines are the same as 5A/mm^2 and 0.4, respectively. Moreover, to accurately compare the

electromagnetic torque ripples, all cogging torque components are removed from electromagnetic torque waveforms. The inner and outer electromagnetic torque waveforms, average values and ripples of three CADMP-FSPM machines are shown in Figs.8 (b), (c) and (d), respectively.

Both inner and outer machines of 10/12-12/22 structure feature the lowest electrical ripples but the highest average torque values, whereas, the average torque values of both inner and outer machines of 5/6-12/22 structure is the lowest as the flux leakage of this structure is the highest.

Among the inner machines, the 5/6-12/22 structure features the highest electromagnetic torque ripples since its inner EMFs suffer from high even-order harmonics. Among the outer machines, the 5/6-18/42 structure features the highest electromagnetic torque ripples as outer EMFs suffer from three-phase asymmetry.

TABLE II Performance of Three CADMP-FSPM Machines

Performance and coupling level	5/6-12/22	10/12-12/22	5/6-18/42
φ_{ave} of inner machine (mWb)	0.85	1.4	0.9
THD of flux-linkage of inner machine (%)	5.27	3.48	11.21
φ_{ave} of outer machine (mWb)	1.4	1.8	A:0.95; B:0.95
THD of flux-linkage of outer machine (%)	4.4	2.47	A: 11.21;B:4.23
EMF per turn of inner machine @1500r/min	0.7V	2.2V	0.73V
THD of EMF per turn of inner machine (%)	41.4	4.5	6.32
EMF per turn of outer machine @600r/min	1.99V	2.5V	A: 2V; B:2.5V
THD of EMF per turn of outer machine (%)	6.2	2.56	A: 30.5; B: 10.2
k_{ripple} of inner machine (%)	5.23	1.66	4.57
k_{ripple} of outer machine (%)	4.46	2.75	3.24
P-P values of cogging torques of inner machines (Nm)	1.40	0.48	1.33
P-P values of cogging torques of outer machines (Nm)	2.29	2.96	49.51
Average values of electromagnetic torques inner machines (Nm)	2.94	4.42	3.33
Average values of electromagnetic torques outer machines (Nm)	9.00	11.75	8.09
Electromagnetic torque ripples of inner machines (%)	58.06	14.82	25.78
Electromagnetic torque ripples of outer machines (%)	39.05	11.02	50.90
Core loss (W)	23.41	38.45	20.33
Efficiency (%)	87.64	90.52	87.70

4.5. Loss and efficiency

The core losses of three CADMP-FSPM machines are shown in Fig. 9. Both inner and outer machines of three CADMP-FSPM machines operate under the rated operation modes together. Moreover, the operation speed and the current density of three inner machines are same as like as three outer machines. The rated operation parameters of three CADMP-FSPM machines are shown in Table III.

Table III The Rated Operation Parameters of Three CADMP-FSPM Machines

	Inner machine		Outer machine	
Structure	5/6	10/12	12/22	18/42
Rotor speed	1500r/min		600r/min	
Current density	5A/mm^2		5A/mm^2	
Slot filling factors	0.4		0.4	
Slot area	169 mm^2	77 mm^2	73 mm^2	52 mm^2
DC bus voltage	380V		380V	

From Figs. 9(a) and (b), 10/12-12/22 structure suffers from the highest core loss as the flux leakage of this structure is the lowest. The core losses of 5/6-12/22 and 5/6-18/42 structures are roughly same as both suffer from high flux leakages.

The core losses of 5/6-12/22 and 5/6-18/42 structures are lower than 10/12-12/22 structure, however, the efficiency of 10/12-12/22 structure is still higher than 5/6-12/22 and 5/6-18/42 structures, as shown in Fig. 9(b). This is because 10/12-12/22 structure features the highest electromagnetic torque whereas the electromagnetic torques of 5/6-12/22 and 5/6-18/42 structures are significantly reduced by flux leakages.

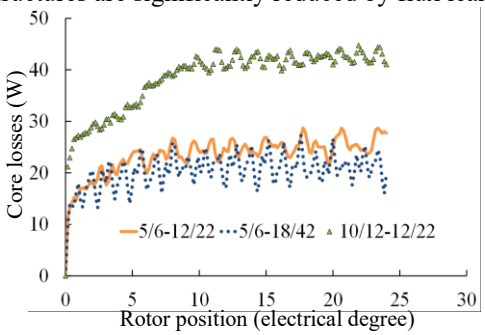

(a)

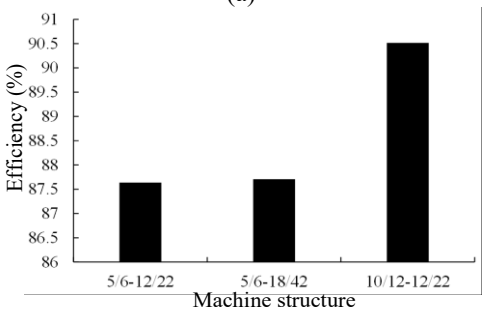

(b)

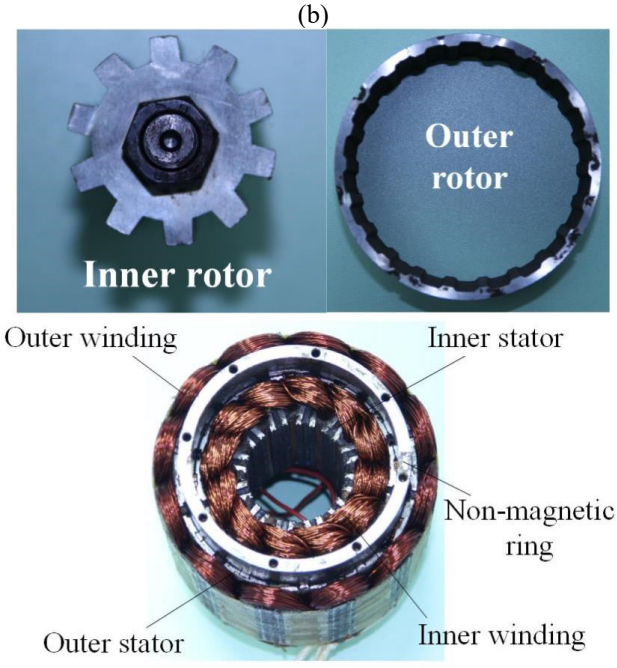

(c)

Fig. 9 *Core loss and efficiencies of three CADMP-FSPM machines and Prototype of a 10/12-12/22 CADMP-FSPM machine.*
(a) Core loss. ***(b)*** Efficiencies. ***(c)*** Inner rotor, outer rotor and Non-magnetic ring & Inner and outer stators.

5. Experimental verifications

5.1. Phase EMF waveforms

A prototyped 10/12-12/22 CADMP-FSPM machine is built, as shown in Fig. 9(c). As can be seen from Figs. 10(a) to (d), both inner and outer machines of 10/12-12/22 structures have avoided the negative effects of PM field coupling.

Both the FEA simulated and experimental EMF waveforms of the inner machine are almost sinusoidal. The EMF amplitudes from the FEA simulations and the experiments of the inner machine are 101V and 94V, respectively, and the error is about 7%, due to the complexity of manufacturing and machine end-effect.

Both the predicted and measured EMF waveforms of the outer machine are also close to sinusoidal. The predicted and experimental EMF amplitudes of the outer machine is 132V and 126V, respectively, with an error about 6%.

The EMF waveforms and amplitudes of experimental and simulation results are shown in Figs. 11(a) and (b). As can be seen, the phase EMF waveforms and amplitudes obtained by FEA simulations and experiments are close. The THDs of inner phase EMF due to experiment and simulation results are 4.92% and 8.60%, respectively. The THDs of outer phase EMF due to experiment and simulation results are 2.82% and 3.65%, respectively. The relative values of individual harmonics of these waveforms are shown in Figs.11(c) and (d), respectively. As can been seen, for the inner machine, the even-order harmonics of experimental result are almost two times higher than that of the simulation, which is due to the imperfect manufacturing. Furthermore, some inner stator teeth have been impacted heavily during the machine assembling, which increase the mechanical error of the inner machine. For the outer machine, the relative values of individual harmonics of experimental and simulation results are close.

5.2. Coupled EMF waveforms

It can be seen from Figs. 12(a) and (b) that the coupled EMF waveforms from both the FEA simulations and experiments of the inner machine are rather small (0.6V for FEA simulation and 0.7V from the experiments), with a rotating outer machine. Again, both the FEA predicted and the measured coupled EMF waveforms of outer machine are also small, being 1.8V and 2V, respectively, with a rotating inner machine. Therefore, the PM field coupling of the optimized 10/12-12/22 CADMP-FSPM machine can be reduced significantly.

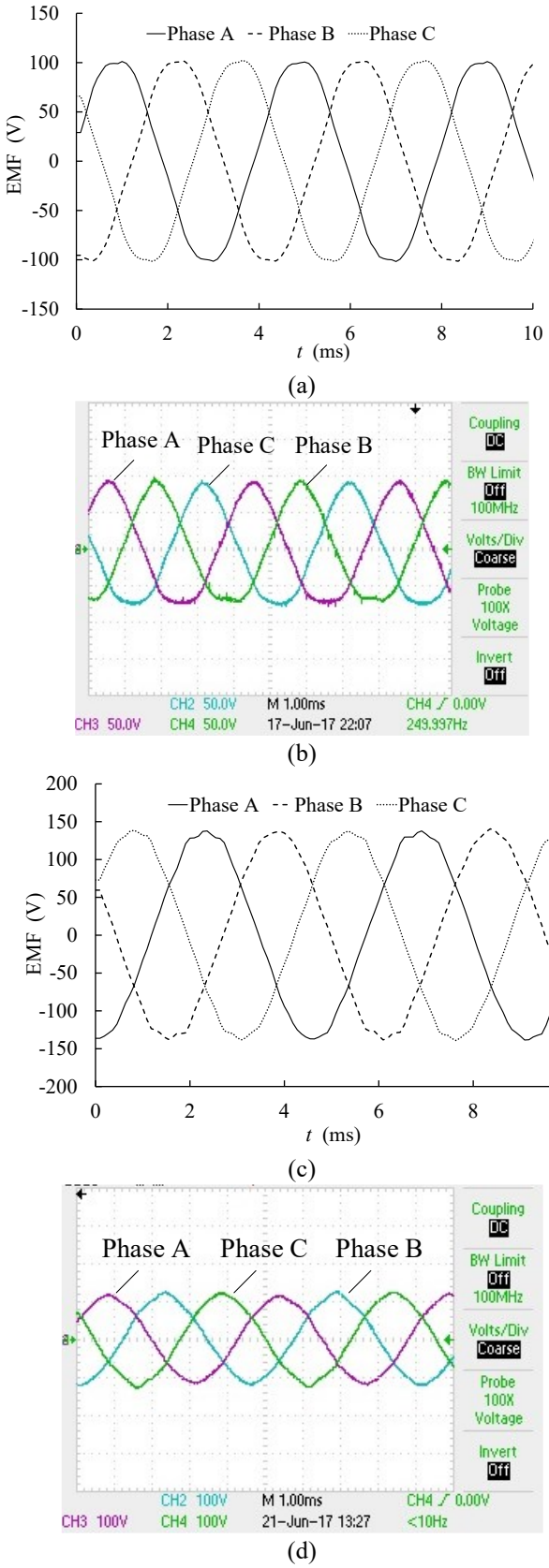

Fig. 10 *waveforms of three-phase EMF of inner and outer machines.*
(a) FEA simulation result of inner machine @1500r/min. ***(b)*** Experiment result of inner machine @1500r/min. ***(c)*** FEA simulation result of outer machine @600r/min. ***(d)*** Experiment result of outer machine @600r/min.

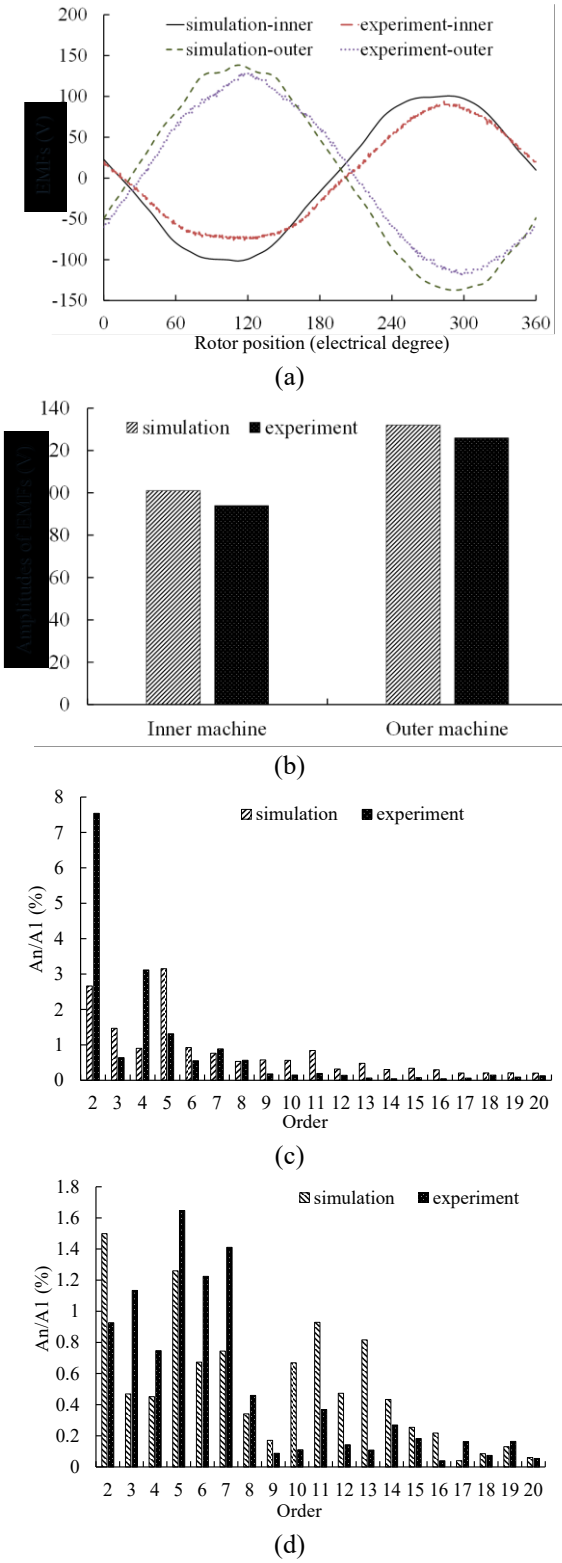

Fig. 11 *waveforms and relative values of individual harmonics of three-phase EMF of inner and outer machines.* ***(a)*** Phase A EMF waveforms of both machines (inner machine @1500r/min, outer machine @600r/min) @1500r/min. ***(b)*** Amplitudes of phase A EMF of both machines (inner machine @1500r/min, outer machine @600r/min). ***(c)*** Relative values of individual harmonics of phase A EMF of inner machine @1500r/min ***(d)*** Relative values of individual harmonics of phase A EMF of outer machine @600r/min.

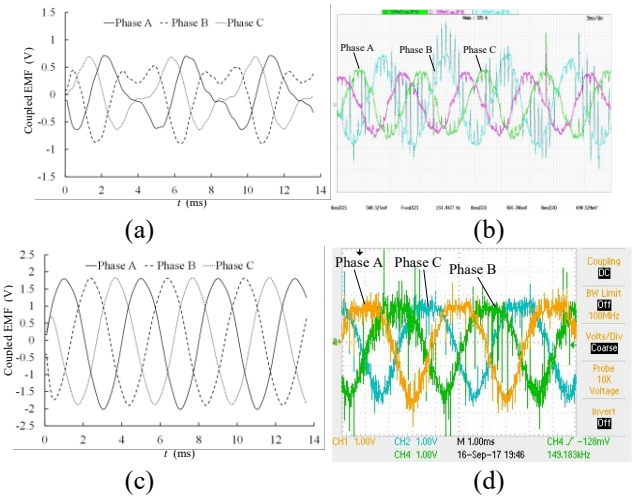

Fig. 12 *Coupled three-phase EMF waveforms of inner and outer machines.*
(a) FEA simulation result of inner machine with a rotating outer machine @600r/min. ***(b)*** Experiment result of inner machine with a rotating outer machine @600r/min. ***(c)*** FEA simulation result of outer machine with a rotating inner machine @1500r/min. ***(d)*** Experiment result of outer machine with a rotating inner machine@1500r/min.

6. Conclusions

In this paper, the PM field coupling between the inner and outer machines of the CADMP-FSPM machine having various stator teeth number collocations is investigated. It is found that the PMs field coupling may cause even-order harmonics of EMF, asymmetric EMF and flux-linkage DC bias component, and all these three problems may degrade the machine performance. Furthermore, the reasons and influence of three problems can be summarized as follows:

1) If the stator teeth types for the same phase windings are different, the air-gap flux density may be unbalanced, which leads to even-order harmonics of EMF. Further, the even-order harmonics not change the average torque but lead to high torque ripple.

2) If the stator teeth types of three phases are different, then, three-phase EMFs are asymmetrical as they feature different flux leakage levels and this asymmetry leads to severe torque ripple and low efficiency. Moreover, series teeth type features the highest flux leakage levels and independent stator teeth type features medium flux leakage. The flux leakages will lead to torque reduction despite of a core loss reduction.

3) If the fluxes of the series magnetic circuits through the phase coils are unidirectional, DC bias components may exist in the phase flux-linkages. Moreover, the peak-to-peak value of cogging torque and torque ripple may be extremely high.

All the analysis above is verified by 5/6-12/22 and 5/6-18/42 structure CADMP-FSPM machines, and the results show both inner and outer stator teeth types should be the same. Therefore, a 10/12-12/22 structure CADMP-FSPM machine having parallel stator teeth in both inner and outer machines is proposed and analyzed. FE analysis results show that the 10/12-12/22 structure features the lowest PM field coupling level and the best performance, which is verified by the experimental results.

7. References

1 B. Powell, and T. Pilutti, “A range extender hybrid vehicle dynamic model,” *Proceedings of IEEE conference of decision and control*, Jul. 1994, vol. 3, pp. 2736-2741.

2 A. Schmidhofer, G. Zhang, and H. Weiss, “Range extender optimization for electrical vehicles,” *Proceedings of IEEE international conference industrial technology*, Oct. 2003, vol. 1, pp. 570-574.

3 F. Yunzhou, Z. Han, P. Qingfeng, et al. “Research on generator set control of range extender pure electric vehicles,” *Proceedings of Asia-Pacific Power Energy conference*, 2010, pp. 1-4,.

4 W. Hua, and L.K. Zhou, “Investigation of a co-axis dual-mechanical-port flux-switching permanent magnet machine for hybrid electric vehicles,” *Energies*, pp. 14364-14379, 2015.

5 E. Hoang, A. H. Benng,, a, J. Lucidarme. “Switching flux permanent magnet polyphased synchronous machines,” *The 7th European Conference on Power Electronic and Applications EPE’97,* 1997, pp. 903-908.

6 Z. Z. Wu, and Z. Q. Zhu. “Analysis of air-gap field modulation and magnetic gearing effects in switched flux permanent magnet machines,” *IEEE Tran. Magn.*, vol. 51, no. 5, pp. 1-12, 2015.

7 Zhu Z Q, Chen J T. “Advanced flux-switching permanent magnet brushless machines,” *IEEE Tran. Magn.*, vol. 46, no. 6, pp. 1447-1453, 2010.

8 Cheng, M., Hua W., Zhang J., et al. “Overview of stator-permanent magnet brushless machines.” *IEEE Trans. Ind. Electron.*, vol. 58, no. 11, pp. 5087-5101, Jan. 2017.

9 L. K. Zhou, and W. Hua, “Power distribution of a co-axis dual-mechanical-port flux-switching permanent magnet machine for fuel-based extended range electric vehicles,” *AIP Advances*, vol. 7, no. 5, paper no. 056638, May 2017.

10 W. Hua, M. Cheng, Z. Q. Zhu, and D. Howe, “Analysis and optimization of back-EMF waveform of a flux-switching permanent magnet motor,” *IEEE Trans. Energy Convers.*, vol. 23, no. 3, pp. 727-733, Apr. 2008.

11 W. Hua, H. Zhang, M. Cheng, et al. “An outer-rotor flux-switching permanent-magnet machine with wedge-shaped magnets for in-wheel light tractions”. *IEEE Trans. Ind. Electron.*, vol. 64, no. 1, pp. 69-80, Jan. 2017.

12 X. Zhu, Z. Shu, L. Quan, et al, “Design and multi-condition comparison of two outer-rotor flux-switching permanent magnet motors for in-wheel traction applications”, *IEEE Trans. Ind. Electron.*, vol. 64, no. 8, pp. 6137-6148, March 2017